ADAPTIVE DEPLOYABLE POLYMER REFLECTORS FOR SMALL SATELLITE APPLICATIONS

Carl Johan Nielsen [(1)], Thomas Godfroid[(2)], Goncalo Rodrigues [(3)], David Alaluf[(3)], Pascal Hallibert[(3)], Michel Géradin[(4)], André Preumont[(1)]

[(1)] Université Libre de Bruxelles, Belgium, Email: carl.nielsen@ulb.be, andre.preumont@ulb.be

[(2)] MateriaNova Mons, Belgium, Email: thomas.godfroid@materianova.be

[(3)] ESA/ESTEC, Netherlands, Email: goncalo.rodrigues@esa.int, david.alaluf@esa.int, pascal.hallibert@esa.int

[(4)] University of Liège, Belgium and TUM Institute for Advanced Study, Germany, Email: mgeradin@gmail.com

ABSTRACT

The paper is a summary of activities in the ESA project Advanced Multilayer Adaptive Thin Shells (AMATS). RFQ/3-17686/22/NL/RA/va. The goal is the development of an actively controlled reflector using piezoelectric polymer materials. The reflector can be folded, deployed, and finally actively controlled.

A metrology system for the measurement of petal-shaped reflectors has been developed based on the Software Configurable Optical Testing System (SCOTS) and verified with raytracing. The SCOTS method is also used to verify the thermal balancing of coupon samples produced by MateriaNova. Finally, numerical viscoelastic simulation is conducted to characterize the expected deployment errors of the reflector.

Introduction

Attaining increased performance of imagining systems is primarily a function of the aperture diameter, which for small satellites is severely constrained. Deployable telescopes are one way to attain larger apertures and thus performance gains in small form factor satellites such as CubeSats. Although most conceptual designs feature rigidly deployable structures such as [1], [2], this paper concerns a foldable piezoelectric polymer actively controlled flexible reflector. The reflector works by sandwiching a piezoelectric PVDF-TrFE layer in between aluminium electrodes on a polymer substrate. When a voltage is applied between the electrodes, the piezoelectric material expands or contracts in the plane, causing a precise deformation of the mirror. The advantage of such a reflector is a simpler deployment mechanism, less mass and highly integrated control. The concept is illustrated in Figure 1. Further, Figure 2 shows the deployment of a passive prototype. Three key issues will be addressed:

1. As shown in Figure 1, the reflector will be cut into segmented petals. This makes in-lab metrology more challenging, and a short review of methods developed in the group to address this will be discussed. The in-lab metrology is based on the Software Configurable Optical Testing System (SCOTS) method, using phase unwrapping techniques suitable for complex domains.

2. The SCOTS methods is further applied to the experimental characterization of the thermal performance of the reflector. The Coefficient of Thermal Expansion of the PVDF-TrFE is significantly higher than the polymer substrate. The reflector must therefore be thermally balanced. The balance is attained by dip-coating, which is a symmetric process. Small coupon samples are tested in balanced and unbalanced configurations.

3. When the reflector is in its stowed state, the polymer substrate will undergo a relaxation process. Subsequent deployment of the reflector will thus be subject to an aberration while the material recovers. A numerical study has been conducted using a nonlinear shell model and viscoelastic material model. The shell geometry is folded, stored, deployed and the expected aberration is investigated to determine the time required before the

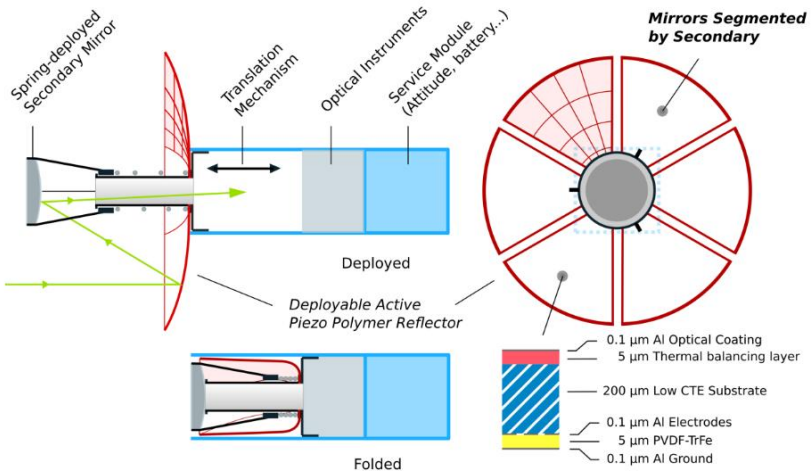

Figure 1 System overview of the deployable reflector telescope. The PVDF-TrFE provides active control, allowing thermal and deployment aberrations to be controlled in orbit.

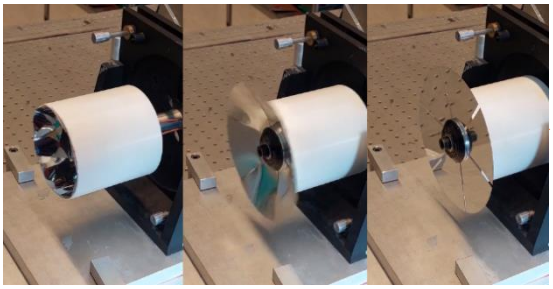

Figure 2 Deployment stages of the polymer reflector. In the experimental setup, the reflector base is stationary while the cylinder moves, to facilitate metrology.

deployment aberration becomes within the control stroke of the PVDF-TrFE active control.

In-lab metrology using modified Software Configurable Optical Testing System

The SCOTS method as envisioned in [3], [4], [5] is a variant of deflectometry, where a camera images the reflection of a known pattern on a test subject in order to determine the shape of the test subject. The test is illustrated in Figure 3. The defining characteristic of SCOTS is the measurement of concave surfaces with camera and pattern near the radius of curvature of the mirror, leading to reduced sensitivity to alignment errors and thus a highly accurate test.

The known pattern is usually a sinusoidal fringe map which is displayed on a PC monitor, and the critical part of the SCOTS test is relating the phase map of the recorded image with the projected image, such that the location of any point on the reflector (Mirror Pixel Location) can be related to any point on the screen (Screen Pixel Location). The step is not trivial, because the phase in any individual point can only be known from $-\pi$ to π unless the whole phase map is considered. Once the relationship is known through phase unwrapping techniques, the vectors $m2c$ and $m2s$ in Figure 3 can be constructed, and from these the slope map of the reflector can be found (or the final shape, with integration).

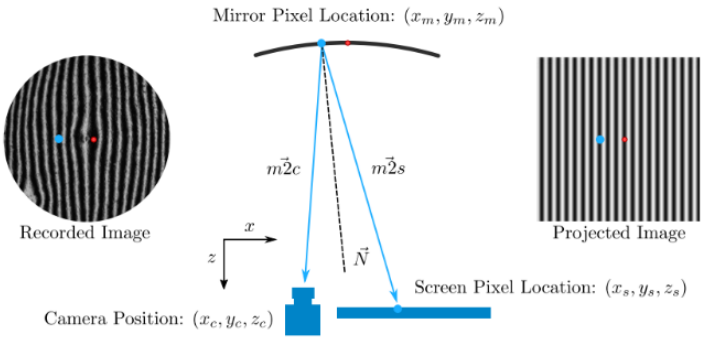

Figure 3 illustration of the SCOTS process. The red dot is the zero-phase location which is determined separately. Once the zero-phase location is known, the two vectors m2c and m2s can be determined by relating points on the recorded image with the projected image.

To allow the measurement of complex geometries, a weighted phase unwrapping technique is used [6] using the petal geometry as a mask. The discontinuity-preserving Mumford Shah integration technique is used to recover the shape from slope data [7].

Using raytracing, the metrology can be tested numerically. First, an aberrated reflector shape is generated by applying a tip displacement in a finite element shell model, leading to a realistic physical shape shown in Figure 4(left). Raytracing of a sinusoidal fringe map reflected in the 3D model, leads to the image in Figure 4(right). By generating several images and using the phase unwrapping algorithm, slope calculation and integration techniques, the shape of the reflector is recovered in Figure 5(left) and the error from the nominal result is shown in Figure 5(right). Further explanations as well as discussion on the assumptions which lead to the small discrepancy (sub-micron) are discussed in [8]. We note that, for the purposes of the polymer reflector study, the accuracy is sufficient and demonstrates the capability to measure the complex geometries in the lab.

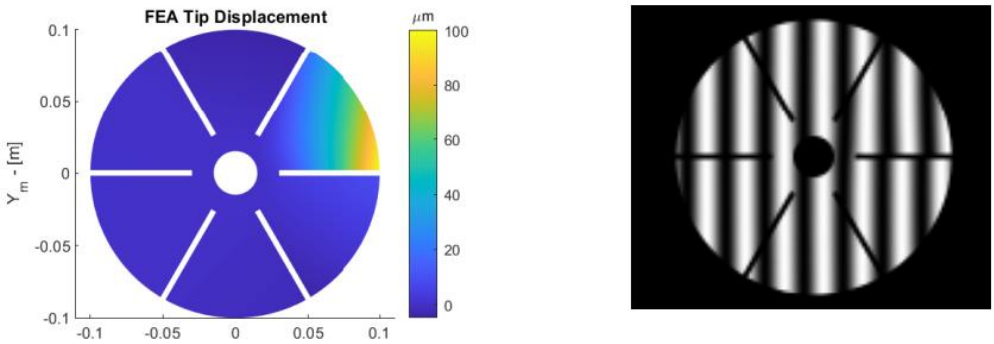

Figure 4 (left) example aberration of the reflector in which a 100 micron tip displacement is applied. (left) raytraced example image of reflected pattern. On the right-hand side, the aberration is apparent by the shifting of the fringes.

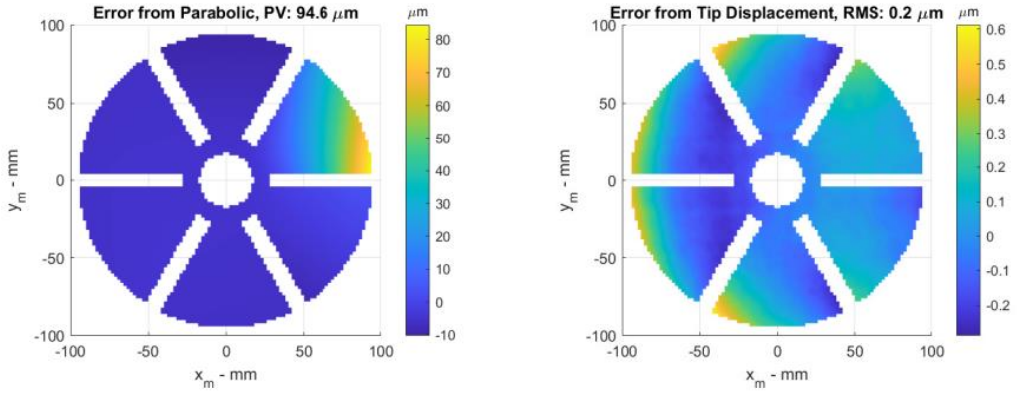

Figure 5 (left) recovered error after phase unwrapping, slope determination and integration. (right) error between applied and measured displacement.

Thermal Balancing of coupon samples

Using the same measurement techniques as explained in the preceding section, the thermal stability is tested on 3 coupon samples in a vacuum chamber under radiative heating on the back side of the samples. The vacuum helps to maintain equal temperature on both sides of the samples, because heat is lost to the environment very slowly (thus, the applied heat is distributed easily in the samples). The concept is illustrated in Figure 6.

1. The top coupon is PEI balanced with Aluminium (Al) on both sides.
2. The middle is unbalanced with Al on both sides and PVDF only on one side.
3. The bottom coupon is balanced with Al and PVDF on both sides.

All coupons have PEI as substrate, with thickness $175\mu m$. The thickness of the PVDF-TrFe layer is $5\ \mu m$. The thermal stability of the top and bottom samples (balanced) is good, whereas the middle sample (unbalanced) is poor.

By imposing the known boundary condition (clamped beam) on the left side of the samples, the shape is reconstructed, and the change in shape is found for all 3 beams.

The results are shown in Figure 7 which suggest a reduction in thermal deformation by a factor of 7 for the balanced sample with PVDF on both sides vs the unbalanced sample.

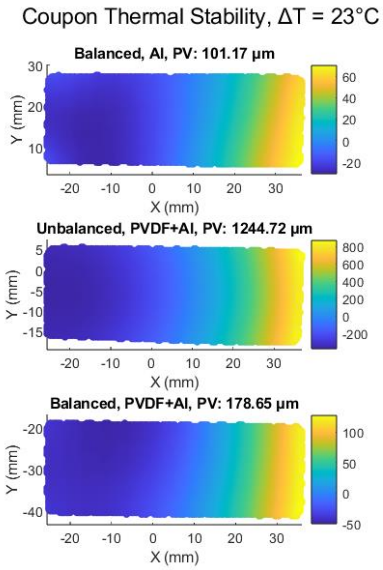

Figure 7 Coupon thermal stability. The thermal deflection of the balanced sample is around 7 times better than the unbalanced sample.

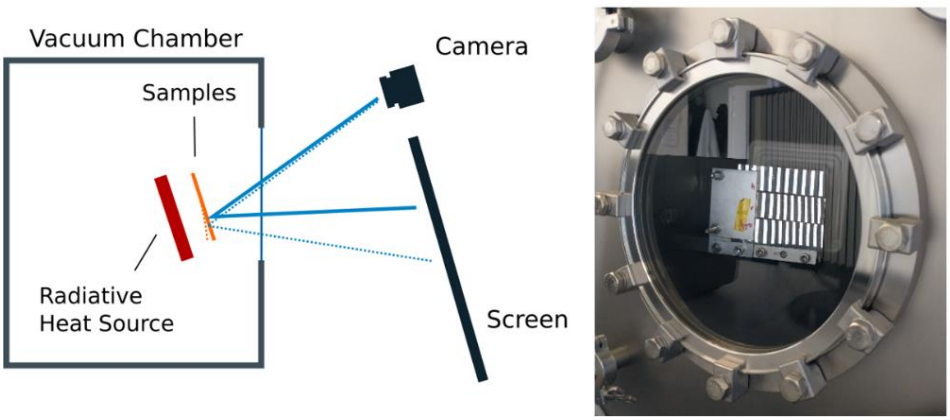

Figure 6 Experimental setup for thermal stability test. When samples are heated uniformly by the radiative source in vacuum, the camera and screen setup can detect small changes in angle. The setup is angled to avoid reflections in the chamber viewport.

Viscoelastic simulation of deployment aberrations

In the stowed state, the polymer substrate material undergoes viscoelastic relaxation from its initial high stress state to a state of lower stress. The internal changes in the material are still present after deployment, and lead to an aberration of the reflector in the unfolded state. The aberration is gradually reduced under viscoelastic recovery where the material recovers to its initial state. The process is reversible only up to a limit of stress, which for the materials considered is around a third of the yield strength [9]. Thus, the first step is to ensure that the material remains below this limit. Subsequently, a viscoelastic model can be implemented. A nonlinear shell model is used for the problem. Figure 8 shows an illustration of the numerical simulation, in which external boundary conditions are applied. The boundary conditions are reduced from a diameter of 20cm to a diameter of 10cm, folding the reflector within the allotted stowed space. Upon folding, the internal stress state can be found, and is shown in Figure 9.

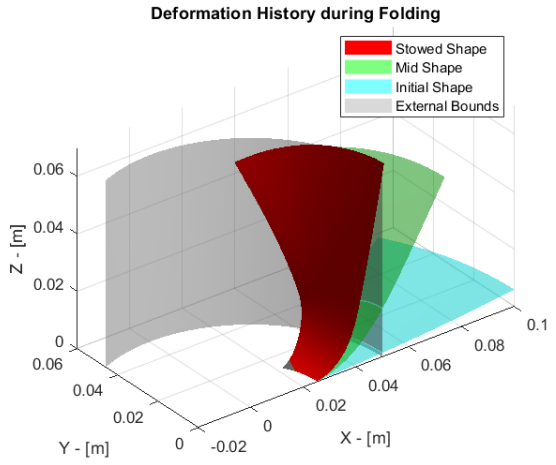

Figure 8 Illustration of the folding stage during numerical simulation. The diameter of the external bounds are gradually reduced, causing the reflector to fold into the stowed state. Half a petal is shown.

The viscoelastic model used is the generalized Maxwell model (Prony series), which is illustrated in Figure 10. The model consists of a spring which governs the long term behaviour of the material, as in a linear elastic material. A series of Maxwell units governs the viscoelastic behaviour on differing timescales. To classify the material, it is necessary to test the properties on many different timescales. For the purpose of this study, we have used just 2 Maxwell units, for which experimental data is available in a relevant timescale [10]. Faster acting Maxwell units are not included, because their contribution in a forced displacement problem can be neglected if only the long-term effects are of importance (the dashpot will quickly relax to a state of 0 stress, and then quickly recover after deployment).

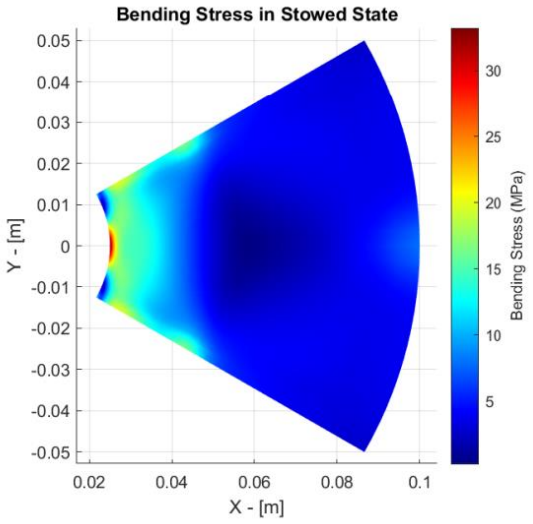

Figure 9 Internal stress state (von Mises bending stress) in the reflector in its folded state. The maximum stress is less than one third of the yield strength, making the use of a reversible viscoelastic model reasonable.

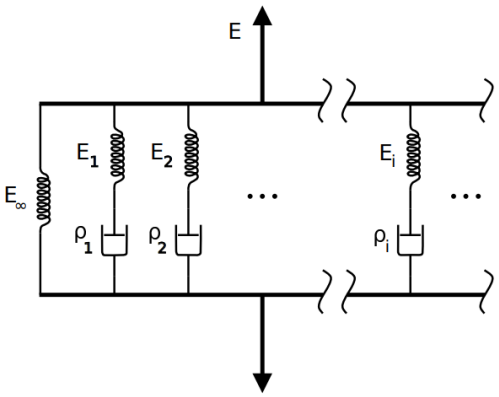

Figure 10 Prony series viscoelastic model of the reflector.

Using material data from [10], the viscoelastic recovery of the reflector is demonstrated in Figure 11. The influence of the temperature is also considered. Following the 24 hours storage, the aberration is relatively quickly recovered. The final step in the process is to consider the control envelope of the reflector, as the voltage applied to the material is limited. In Figure 12, the influence functions of each individual electrode is calculated in FEM, and used to model the control of the reflector. A best fit correction is found, and the residual error and electrode voltages are found.

For the examples viscoelastic aberration, the electrode control voltage are well within the range of control, which for practical purposes is on the order of 300V. For aberrations of this magnitude, the residual error is still outside the range of operation in the visible or Long Wave Infrared (LWIR) wavelengths. However, it is well within the range of control with MEMS adaptive mirrors.

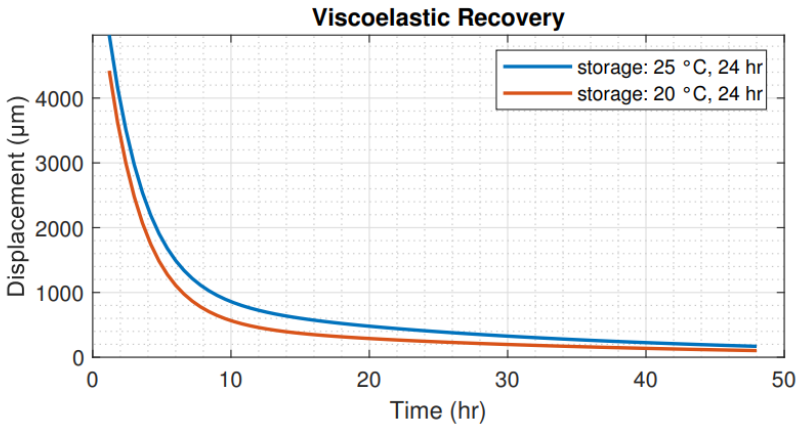

Figure 11 Viscoelastic recovery of the reflector after storage at 2 different temperatures. 2 Maxwell units in material model.

The numerical simulations were performed using a viscoelastic shell finite element and a contact algorithm specifically developed and implemented in the JuDyn software [11] in support to this project.

Conclusion

The in-lab metrology, thermal stability and viscoelastic deployment has been considered for the actively controlled piezoelectric polymer reflector. It was shown that metrology is feasible using a variation of the SCOTS test. Raytracing allows for a full numerical simulation of the metrology, and with assumptions explained in [8] a sufficiently low aberration is demonstrated.

The SCOTS test was also used to explore the thermal stability of coupon samples before scaling the dip-coating process to the full reflectors. A 7 times reduction in the bending of samples was demonstrated with a balanced PVDF-TrFE layer as opposed to a single-sided configuration.

Finally, the numerical simulation of the folding indicated stresses less than a third of the substrate materials yield strength, indicating a reversible viscoelastic model is applicable. Simulation of stowage and deployment (relaxation and recovery) shows that the aberration drops to an aberration of 100 microns after 2 days, which is within the control envelope of the PVDF-TrFE.

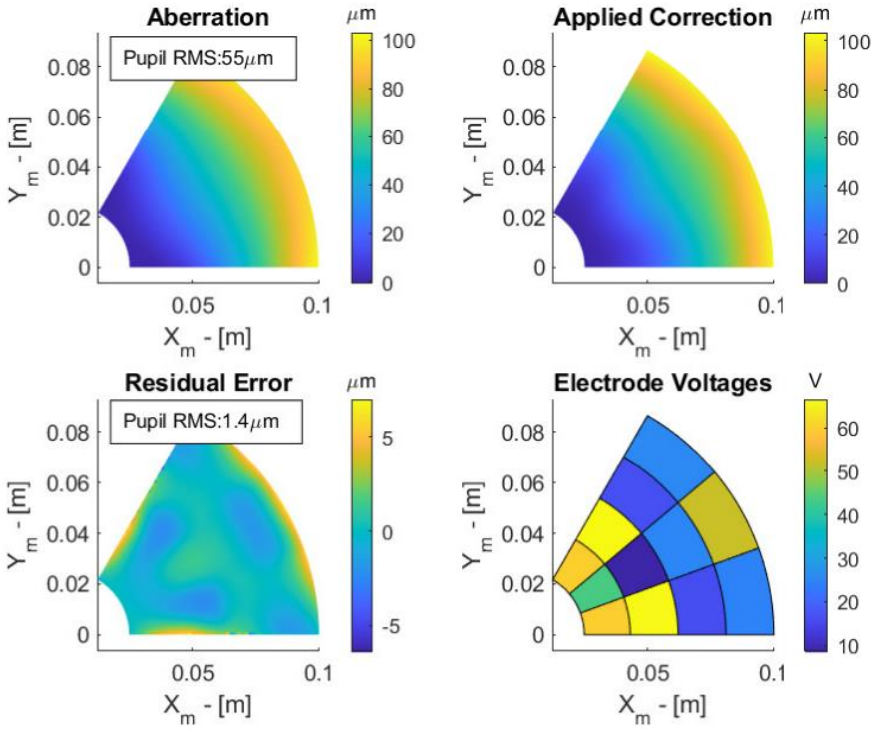

Figure 11 Active control of the reflector from the viscoelastic deployment aberration. Control voltages are well within the range of control, and residual errors are within the range of MEMS AO.

References

[1] J. A. Champagne, S. M. Hansen, T. T. Newswander, and B. G. Crowther, ‘CubeSat Image Resolution Capabilities with Deployable Optics and Current Imaging Technology’.

[2] N. Schwartz *et al.*, ‘High-resolution deployable CubeSat prototype’, in *Space Telescopes and Instrumentation 2020: Optical, Infrared, and Millimeter Wave*, SPIE, Dec. 2020, pp. 565–577. doi: 10.1117/12.2562255.

[3] P. Su, R. E. Parks, L. Wang, R. P. Angel, and J. H. Burge, ‘Software configurable optical test system: a computerized reverse Hartmann test’, *Appl. Opt.*, vol. 49, no. 23, p. 4404, Aug. 2010, doi: 10.1364/AO.49.004404.

[4] J. H. Burge, P. Su, G. Butel, R. Huang, A. Maldonado, and T. Su, ‘Measuring large mirrors using SCOTS: the Software Configurable Optical Test System’, in *Advances in Optical and Mechanical Technologies for Telescopes and Instrumentation*, SPIE, Jul. 2014, pp. 311–323. doi: 10.1117/12.2057726.

[5] A. E. Lowman, G. A. Smith, L. Harrison, S. C. West, and C. J. Oh, ‘Measurement of large on-axis and off-axis mirrors using software configurable optical test system (SCOTS)’, in *Advances in Optical and Mechanical Technologies for Telescopes and Instrumentation III*, SPIE, Jul. 2018, pp. 405–418. doi: 10.1117/12.2313855.

[6] D. C. Ghiglia and L. A. Romero, ‘Robust two-dimensional weighted and unweighted phase unwrapping that uses fast transforms and iterative methods’, *JOSA A*, vol. 11, no. 1, pp. 107–117, Jan. 1994, doi: 10.1364/JOSAA.11.000107.

[7] Y. Quéau, J.-D. Durou, and J.-F. Aujol, ‘Variational Methods for Normal Integration’, Sep. 18, 2017, *arXiv*: arXiv:1709.05965. doi: 10.48550/arXiv.1709.05965.

[8] C. J. G. Nielsen and A. Preumont, ‘Adaptive Petal Reflector: In-Lab Software Configurable Optical Testing System Metrology and Modal Wavefront Reconstruction’, *Sensors*, vol. 23, no. 17, Art. no. 17, Aug. 2023, doi: 10.3390/s23177316.

[9] J. Jansons, A. Aniskevich, and L. Pazhe, ‘Analysis of reversible and irreversible strains in the creep of a nonlinear viscoelastic polymer’, *Mech. Compos. Mater.*, vol. 48, no. 2, pp. 209–216, May 2012, doi: 10.1007/s11029-012-9266-6.

[10] A. Allen, A. Mashin, and K. Kwok, ‘Onset of Creasing in Polymer Thin Membranes’, in *AIAA SCITECH 2022 Forum*, in AIAA SciTech Forum. , American Institute of Aeronautics and Astronautics, 2021. doi: 10.2514/6.2022-1882.

[11] M. Géradin, *JuDyn : a Julia package for flexible multibody dynamics*. (2024). [Online]. Available: https://github.com/michelg45/JuDyn.jl